Dynamics of a bacterial multidrug ABC transporter in the inward- and outward-facing conformations.

Shahid Mehmood, Carmen Domene, Eric Forest, Jean-Michel Jault

Dynamics of a bacterial multidrug ABC transporter in the inward- and outward-facing conformations

Shahid Mehmood[a,b,c], Carmen Domene[d], Eric Forest[a,b,c,1], and Jean-Michel Jault[a,b,c,1]

[a]Institut de Biologie Structurale, Université Joseph Fourier Grenoble 1, 38027 Grenoble Cedex 1, France; [b]Commissariat à l'Energie Atomique et aux Energies Alternatives Grenoble, 38027 Grenoble Cedex 1, France; [c]Unité Mixte de Recherche 5075, Centre National de la Recherche Scientifique, 38027 Grenoble Cedex 1, France; and [d]Department of Chemistry, Physical and Theoretical Chemistry Laboratory, University of Oxford, Oxford OX1 3QZ, United Kingdom

The study of membrane proteins remains a challenging task, and approaches to unravel their dynamics are scarce. Here, we applied hydrogen/deuterium exchange (HDX) coupled to mass spectrometry to probe the motions of a bacterial multidrug ATP-binding cassette (ABC) transporter, BmrA, in the inward-facing (resting state) and outward-facing (ATP-bound) conformations. Trypsin digestion and global or local HDX support the transition between inward- and outward-facing conformations during the catalytic cycle of BmrA. However, in the resting state, peptides from the two intracellular domains, especially ICD2, show a much faster HDX than in the closed state. This shows that these two subdomains are very flexible in this conformation. Additionally, molecular dynamics simulations suggest a large fluctuation of the Cα positions from ICD2 residues in the inward-facing conformation of a related transporter, MsbA. These results highlight the unexpected flexibility of ABC exporters in the resting state and underline the power of HDX coupled to mass spectrometry to explore conformational changes and dynamics of large membrane proteins.

ATPase cycle | structural biology | detergent

Import of nutrients and export of signaling molecules or noxious compounds are essential processes for life, and selectivity for crossing membrane is usually governed by dedicated transporters. The ATP-binding cassette (ABC) is one of the largest families of transporters involved in these "checkpoints." They are found in all living species and use ATP hydrolysis to transport a wide variety of substrates (1). The dysfunctions of several ABC transporters cause severe pathologies, such as adrenoleukodystrophy, hyperinsulinemic hypoglycemia, or cystic fibrosis (2). Other medically important ABC transporters are responsible for multidrug resistance (MDR) phenotypes. Multidrug transporters are capable of recognizing and expelling many unrelated organic compounds with quite dissimilar chemical scaffolds. Thus, although their original function is to protect healthy cells, the occurrence of these transporters in malignant tissues, pathogenic microorganisms, or parasites confers a resistance toward the curative drugs. The archetype of multidrug ABC transporters is the human MDR1 (or ABCB1); it is responsible for the failure of chemotherapeutic treatments in cancerous tissues. In bacteria, the identification of related transporters is relatively recent, compared with other families of multidrug transporters that use the proton gradient as the energy source (3). However, growing bodies of evidence support the implication of these multidrug ABC transporters in antibiotic resistance in many species, jeopardizing a successful therapy (4).

All ABC transporters share a common architecture, with two transmembrane domains (TMDs) responsible for substrate translocation and two nucleotide-binding domains (NBDs). In most exporters, these four domains are either linked into a single polypeptide or function as dimers with one NBD fused to one TMD (homo- or heterodimers). As opposed to the TMDs, the NBDs are highly conserved, with several distinctive motifs, notably the Walker A and Walker B found in many ATPases and the ABC signature specific to this family (5, 6). NBD structures

have shown that during the catalytic cycle, the two NBDs interact transiently to form a sandwich dimer in a head-to-tail fashion, thereby trapping two ATP molecules at their interface (7–9). In this closed conformation, which can be stabilized either by ATPase-inactive mutations (10) or by vanadate-induced ADP trapping (11), each composite ATP-binding site is made of elements from one NBD (i.e., Walker A and B motifs), whereas the ABC signature is provided *in trans* by the second NBD. The overall structure of exporters is less compact than that of importers with two large intracellular domains (ICDs), ICD1 and ICD2, which protrude from the TMD to interact with the NBD. Importantly, whereas ICD1 from one monomer interacts with its own NBD, ICD2 (or ICD4 for full-length exporters) interacts mainly with the NBD of the other monomer (or other moiety) (12–14), and this has been validated by cross-linking experiments (15, 16). Snapshots of 3D structures and electron paramagnetic resonance (EPR) spectroscopy suggest that large motions occur during the catalytic cycle of ABC exporters, with the transporter oscillating between an apo, open (or inward-facing), conformation, with its two NBDs lying far apart, and an ATP-bound closed (or outward-facing) conformation, with the NBDs engaged in a tight interaction (12–14, 17). However, the open structures have raised some skepticism and were proposed to reflect nonphysiological states of the proteins, possibly induced by the presence of detergent (18, 19). Importantly, in all of the structures solved, the contacts between ICDs and NBDs are always maintained, because these two domains keep the same overall conformation and interactions. This suggests that NBD closure operates by a rigid body motion (12, 14). On the other hand, cross-linking experiments between ICDs and NBDs give support to alternative conformations for these two domains in different ABC exporters (15, 16, 20, 21).

To shed light on structural modifications that might occur during the mechanism of ABC transporters, we used a hydrogen/deuterium exchange (HDX) approach coupled to mass spectrometry (MS). HDX has been widely used on soluble proteins to probe the accessibility of backbone amides, thus highlighting secondary structure modifications at the peptide level (22, 23). For membrane proteins, this approach is only beginning to emerge (24–26), but its usefulness has been demonstrated, for example, to pinpoint the conformational changes associated with the binding of ligands, agonists, or antagonists, to the β-2-adrenergic receptor GPCR (27). Given the importance of membrane proteins, our results emphasize the benefit of using HDX to address fundamental issues about their functioning. Here, it revealed the dynamics of a multidrug transporter homologous to

MsbA, Sav1866, and to murine MDR1 (28, 29). In particular, it showed that the two ICDs of BmrA behave quite differently, depending on the conformational state considered, and are unexpectedly highly flexible in the resting state. These results extend our vision of the functioning mechanism of ABC exporters and complement the snapshots of the catalytic cycle acquired from high-resolution 3D structures.

Results

BmrA Switches Between Two Opposite Conformations. 3D structures of ABC exporters solved in the presence of detergent have suggested that large conformational changes might occur during the ATPase cycle (12, 14). To investigate this, we checked whether the presence of detergent affected the conformational changes that take place during the catalytic cycle of BmrA. In agreement with our previous results (30), the ATPase activity of BmrA was conserved in a detergent solubilized state and sensitive to vanadate inhibition (Fig. S1). Then, global HDX was performed on the protein either purified in detergent or in a membrane environment previously shown to preserve the functional state of the transporter (29). The deconvoluted masses obtained from electrospray of BmrA, either embedded in membrane ($66,341 \pm 3$ Da) or purified in n-dodecyl-β-D-maltoside (DDM) ($66,339 \pm 3$ Da), are in very good agreement with the theoretical mass of BmrA, possessing only one extra Ser amino acid on its N terminus (66,340 Da; Fig. S2). The other peaks of lower intensity were due to sequence heterogeneity (*SI Results*) and unidentified noncovalent adducts on both forms of BmrA.

After incubation of BmrA preparations in deuterated buffers, the mass of deuterated BmrA was measured. The percentage of deuterated amides was calculated, taking into account the average of total number of amide hydrogens in BmrA (585 for the native protein) and the mass increase. Curves for deuteration kinetics show the same behavior, with the exchange steadily increasing with time for BmrA in both states (Fig. 1). However, BmrA in membranes was approximately half less deuterated (13–23%) than in its solubilized form (23–47%). This lower deuteration exchange in membrane could possibly reflect a more compact conformation of the BmrA dimer. However, when the same experiment was performed after prior incubation of BmrA with vanadate in the presence of ATP-Mg (closed symbols in Fig. 1) [i.e., conditions known to promote the formation of a closed dimer (11)], a lower deuteration level was found for BmrA either in
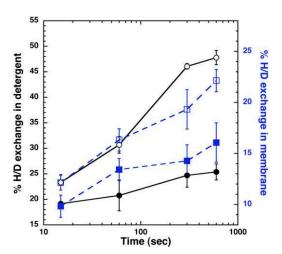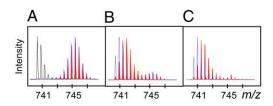
membrane (squares in Fig. 1) or in detergent (circles in Fig. 1). Thus, although HDX occurs at approximately twice the rate in detergent compared with the membrane-bound BmrA, vanadate inhibition induced a significant decrease in HDX, to a similar extent for both environments. Therefore, this shows that in either state, BmrA can switch between two different conformations: an apo one whereby deuterium exchange readily occurs and a closed one more resistant to deuterium exchange.

To bring further evidence for the similar behavior of BmrA in detergent and membranes, limited digestion with trypsin was carried out. BmrA in the apo conformation was rapidly digested by trypsin in membranes as well as in DDM (Fig. S3). In contrast, in the closed conformation (+Vi), BmrA was quite resistant to this protease in both environments. Thus, regardless of its environment, BmrA adopts two different conformations with opposite sensitivity to trypsin.

Peptide Mapping of BmrA. To achieve a sequence coverage as large as possible, local HDX was performed on purified BmrA because (*i*) a much higher deuteration level was found for the protein in detergent, and (*ii*) the presence of *Escherichia coli* proteins in the membrane fraction would hamper the unambiguous identification, or the determination of deuterium incorporation, for some BmrA peptides. Optimized conditions led to a sequence coverage of 78% using pepsin (Table S1). It was lower in the TMD (60%), with the majority of the identified peptides belonging to the hydrophilic ICDs, ICD1 and ICD2 (Fig. S4). In contrast, the NBD sequence was almost fully covered by the pepsin digestion (98%). Because deuteration induced the spreading of isotopic envelopes (i.e., the ensemble of isotopic peaks of a peptide), it often led to signal decrease and overlapping. Thus, a significant number of peptides were lost after deuteration, giving 45% and 92% coverage for TMD and NBD, respectively. Importantly, most of the two ICDs were still covered by HDX because these two subdomains are essential for the transmission of the conformational changes between the NBD and the TMD (13, 31, 32).

Comparison of the Closed Forms of BmrA Using HDX. Besides the inhibition by vanadate, another way to promote the closed conformation in ABC transporters is to use catalytic inactive mutants (8, 9, 33). For BmrA, we previously showed that the conserved glutamate residue E504 adjacent to the Walker B motif is very likely the catalytic base for ATP hydrolysis, because mutation of this residue fully abrogated the activity (10, 34). Deuterium incorporation was monitored as a function of time and was compared for each peptide generated from the three following forms of BmrA: wild-type in the resting state (apo form), wild-type inhibited by vanadate (in the presence of ATP-Mg), and E504A mutant in the presence of ATP-Mg (Fig. S5). In some cases (e.g., in Fig. 2), spectra from the vanadate-inhibited form showed two envelopes of isotopic peaks, thus giving two different kinetics, with the minor envelope corresponding to that

Fig. 1. Global deuteration kinetics of BmrA. HDX was followed for BmrA in membranes (squares) or purified in DDM (circles), either in the resting state (open symbols) or in a vanadate-inhibited state (filled symbols). SDs for two separate experiments are shown.

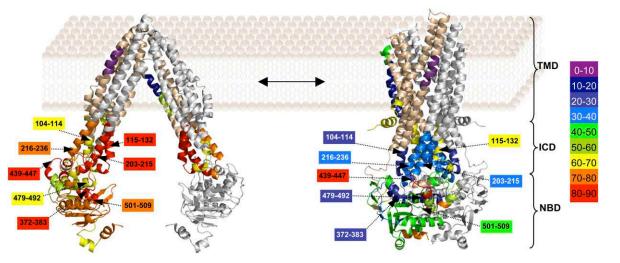**Fig. 2.** Isotopic profiles of 203–215 peptide at two deuteration times. The mass spectra of peptide 203–215 from ICD2 is shown before (black peaks) or after 15 s (blue peaks) and 3,600 s (red peaks) of deuteration. This peptide was from the wild-type BmrA in the resting state (*A*) or vanadate-inhibited state (*B*) or from the E504A mutant incubated in the presence of ATP (*C*).

BIOCHEMISTRY

of the wild-type in the apo form. Presumably, this envelope originates from BmrA dimers not inhibited among the whole population, because the inhibition of ATPase activity by vanadate was not total (~80%; Fig. S1) (see also refs. 17 and 30). In contrast, the E504A mutant showed practically only one isotopic envelope that was always similar to that of the low molecular mass observed in the vanadate-inhibited sample. Given the propensity of the E504A BmrA mutant to readily adopt the closed conformation of BmrA in the presence of ATP-Mg, and the homogeneity of HDX of its peptides, we focused on the differences between this mutant in the closed conformation (ATP-bound state) and the wild-type in the apo conformation (resting state).

Influence of the BmrA Conformation on HDX of the ICDs and NBDs. The major differences in HDX between both forms can be visualized on the "heat map" presented in Fig. S6. The regions in red or orange correspond to peptides with more than 45% and 30% HDX difference, respectively, after 1 h deuteration. They clearly belong to ICD1, ICD2, and the NBD, particularly the Walker A motif and the ABC signature, which are known to be involved in nucleotide binding. To highlight the HDX data, two BmrA models (28) based on the X-ray structures of homologous bacterial ABC transporters were used (Fig. 3). For the apo conformation of BmrA, the open structure of EcMsbA was used as a template, whereas the closed conformation of BmrA (mimicked by the ATP-bound E504A mutant) was modeled on the Sav1866 structure (13, 14). In agreement with the closed model, the regions participating in either NBD dimerization or direct interaction with ATP/Mg show a rather low level of HDX. This is the case, for instance, for the peptide 372–383, which entirely covers the Walker A motif (HDX of 29%), or for the peptide 479–492 encompassing the ABC signature (26%). In contrast, the former peptide became much more rapidly deuterated in the apo conformation with a high deuteration level of the Walker A motif (82%), consistent with the presence of a large accessible loop, whereas the peptide covering the ABC signature motif also showed a substantial increase in its exchange rate (69%). The lowest value of HDX obtained for this second peptide suggests that in the open conformation, the region likely conserved an α-helical structure less prone to HDX than a loop. Thus, the exchange rates for these two peptides are in agreement with the open model used to depict the apo conformation

(Fig. 3). For other peptides of the NBDs known to be involved in ATP binding or NBD dimerization, similar trends were observed, with a faster exchange rate in the apo conformation compared with the ATP-bound conformation (e.g., peptide 501–509 including most of the Walker B motif). Other regions of the NBDs not involved in either process gave similar HDX in both conformations with, for instance, a high deuteration level consistent with a loop structure (84%) for peptide 439–447.

A different picture emerges when one focuses on ICDs. In contrast to the two models suggesting that these domains have a similar conformation in the two states, open and closed, peptides from both ICDs showed a large difference in the HDX in these two conformations. Thus, ICD2 was highly deuterated in the apo conformation, with 82% and 79% for peptides 203–215 and 216–236, respectively, whereas in the closed conformation the HDX rate significantly decreased to 33% and 34%, respectively. Likewise, but to a lower extent, regions 104–114 and 115–132 from ICD1 were also fairly deuterated in the apo conformation (66% and 81%, respectively). This value dropped to 27% in the closed state for the former peptide, whereas it remained highly deuterated for the latter (69%). Because the solvent accessibility of amide hydrogens from both ICDs is essentially unaffected upon the dimerization of the two NBDs (e.g., for peptides 104–114 and 203–215) (Fig. S7), the much faster rate of HDX observed in the resting state for these peptides must reflect a modification of conformation and/or flexibility of each ICD. It must be noted that in the closed state, some residues of ICD1 interact with ICD2 within the same subunit (see ref. 13) and thus will help to restrict the motion of the two ICDs.

To further assess the flexibility of these two domains in the 3D structures of the related transporters used to model BmrA, molecular dynamics simulations of ~100 ns were performed on EcMsbA and Sav1866, along with that of StMsbA that was included for comparison. After reaching a plateau for the rmsd of the Cα for each conformation, the fluctuation of the position of the Cα atoms were calculated for the last 20 ns of the trajectories, and the results are shown in Fig. S8. Clearly, a minor fluctuation was observed in the closed conformations of either Sav1866 or StMsbA, regardless of the Cα considered (always below 2.5 Å). In contrast, some basal fluctuations occurred throughout the sequence of EcMsbA and were much more pronounced (above 4 Å) for four areas, including in particular ICD2. This suggests that this latter domain must be quite flexible in this apo conformation.

Fig. 3. HDX of peptides using BmrA 3D models. 3D models of BmrA in the open conformation (*Left*) or in the closed conformation (*Right*). One subunit was drawn in wheat color and the other in light gray. Identified peptides are drawn with rainbow colors (in one monomer and in all ICDs) according to their percentage of deuterium exchange after 3,600 s (scale of exchange shown at right). Selected regions are also shown with arrows.

Mehmood et al.

Discussion

The goal of this study was to get insights into the dynamics of a multidrug ABC transporter in two different conformations: the resting state, in which the transporter adopts presumably an open conformation (the extent of which remains to be determined), and the closed state, in which the two NBDs dimerize in a transient, ATP-bound, conformation. Overall, global HDX and trypsin digestion show that either in membrane or in detergent, BmrA can switch between two very different conformations during its catalytic cycle: a closed form rather resistant to trypsin digestion and HDX, and another one in the resting state quite sensitive to trypsin and more susceptible to HDX. Thus, our results support the postulate that multidrug ABC transporters can cycle between an open, inward-facing, conformation in the resting state and a closed, outward-facing, ATP-bound conformation. Similar conclusions were drawn for the catalytic cycle of MsbA from cross-linking experiments (35) or from EPR spectroscopy (17, 36, 37). On the basis of 3D structures of ABC exporters, the transition between these two opposite conformations was proposed to operate according to a rigid body motion (14). This entails that the same overall structure of the two monomers (or moieties for full-length transporters) would be maintained throughout the catalytic cycle. However, local HDX obtained for BmrA clearly challenges this assumption and suggests that in the resting state, BmrA samples different conformations. However, these different conformations seem to be restricted to both ICDs. Indeed, apart from the peptides involved either in the interactions between the two NBDs or with ATP, no major changes are observed for the other peptides from either the NBD or the transmembrane helices, although limited information is available for the latter. Therefore, the interaction between the TMD and the NBD that is secured by the two ICDs in the closed state must become loose in the resting state owing to a greater flexibility of these ICDs. This would allow some reorientation of the whole NBD compared with the TMD and would explain some unexpected cross-links previously observed for BmrA. It was found that disulfide bonds were formed between ICD1 and the Q-loop of the NBD in the resting state only (20). However, in all structures of exporters, either closed or open, ICD2 is sandwiched between ICD1 and the Q-loop, thereby impeding the possible interaction between these two protein segments (12–14). Hence, some reorganization of BmrA domains would be required to allow the cross-link between ICD1 and the Q-loop (20). Other unpredicted cross-links questioning the conformation observed in 3D structures were also reported for two other ABC transporters, TAP1/TAP2 and Yor1p (15, 21). These results lend support to additional conformations of these transporters, with different orientations of the NBD relative to ICDs or of the two ICDs with respect to each other. Other studies performed on homodimeric ABC transporters, LmrA and MsbA, using either solid-state NMR or EPR spectroscopy, reached similar conclusions of alternative conformations (or greater flexibility) of the NBD in the resting state, as opposed to the TMD (36, 38). In addition to the NBD flexibility, EPR experiments also support a large conformational entropy of residues from ICD1 in the resting state, as evidenced by the large distance distribution of the spin label probe tethered to residue 115 of MsbA (36). Unfortunately, the flexibility of ICD2 could not be tested because the tethering of a spin probe to cysteine residues in this domain was detrimental to MsbA activity (37). For the cystic fibrosis transmembrane conductance regulator (CFTR), although cross-link patterns support a global architecture similar to that found in Sav1866 or MDR1, a considerable flexibility at the interface of NBDs and ICDs was proposed to explain the formation of cross-links between these two domains, even with long cross-linker reagent (up to 24.7 Å) (16). In addition, a recent report using a genetic screen with the yeast ABC multidrug transporter PDR5 supports the idea of a noncanonical coupling between the NBD and the TMD as being mainly achieved through ICD1 and not through ICD2 (39).

Whether this is a peculiar property of PDR5 or reflects an alternative conformation of the ICDs remains to be investigated. Interestingly, a molecular dynamics study of Sav1866 indicated that in a closed conformation and among residues whose Cα show the largest displacement between the ATP and ADP+Pi bound states, some belong to ICD2 (residues 221–222) and to ICD1 (residues 110–113) (40). Here, molecular dynamics simulations suggest that in the apo conformation of EcMsbA, large fluctuations in the positions of the Cα atoms of ICD2 would take place. Conformational flexibility, and in particular of α-helices, has been reported for some membrane proteins, such as the lactose permease (41, 42), the osmoprotectant symporter ProP (43), and the glycerol facilitator (44), and this property likely pertains to the transport of their respective substrates (45). For multidrug ABC transporters, the flexibility of ICDs might not only be involved in the transport mechanism but possibly also permits the polyspecificity of drug recognition, provided that this flexibility could be propagated to the drug-binding site(s).

HDX coupled to MS is commonly used to probe the dynamics of soluble proteins, but this technique remains artful in the case of membrane proteins, especially because detergent often reduces the sequence coverage. Up to now, the only ABC transporter for which this technique was used was the soluble NBD1 of CFTR (46). However, our results on BmrA emphasize how useful this technique is, especially to study membrane proteins with large extramembranous domains. This includes, for example, secondary transporters of the resistance-nodulation-cell division family, such as AcrB (47), or primary transporters of the P-type family like the Ca²⁺-ATPase (48). The use of HDX coupled to MS to unravel different conformations of these membrane proteins should shed new light on their transport mechanism.

Materials and Methods

Site-Directed Mutagenesis and Purification of BmrA. The E504A BmrA mutant was constructed as previously described (10). The E504A mutant and wild-type BmrA were overexpressed as previously described (49), and BmrA-enriched membranes were either frozen in liquid nitrogen and kept at −80 °C until used or solubilized in 1% DDM. After solubilization, BmrA was purified by Ni-affinity chromatography as previously described (29).

HDX of BmrA. The HDX reaction was initiated by a 10× dilution into deuterated buffer containing 50 mM NaCl and 0.05% DDM. Time course of the HDX was followed over a 1-h period by sequential withdrawing of 120 μL deuterated samples, which were immediately added to 26 μL of quenching buffer (8 M guanidium chloride, 500 mM glycine HCl, pH 2.2), rapidly mixed, and flash-frozen in liquid nitrogen.

HPLC Peptide Separation. After protease digestion in solution or on-column in an ice bath at 0 °C, peptides were loaded onto a peptide MicroTrap (Michrom Bioresources) column and washed with 0.03% TFA in water (HPLC solution A). They were then separated on a reversed-phase C12 column (1 × 50 mm, Jupiter; Phenomenex) using a linear gradient of 15–45% (vol/vol) solution B (CH₃CN 95% and TFA 0.03%) during 26 min. The column was connected to the electrospray source of mass spectrometers until 30% (vol/vol) B and then disconnected to avoid pollution of the electrospray source by the detergent. The valves, trap cartridge and column were cooled to 0 °C by immersion in an ice bath.

Mass Spectrometric Analyses of Peptides. The tandem MS (mapping) analyses were performed on an ion trap mass spectrometer (Esquire 3000+; Bruker Daltonics) to enable the identification of the peptides after their separation on HPLC. Accurate mass measurements and the analysis of the local kinetics of deuteration were done on a time-of-flight (TOF) mass spectrometer (6210; Agilent Technologies) equipped with an electrospray source. Data were processed with MassHunter Qualitative Analysis, and the deconvolution and calculation of the average masses were carried out in Magtran (50).

Electrospray Mass Spectrometry of the Full-Length Protein. The molecular mass of the intact protein was measured with the same electrospray TOF mass spectrometer coupled with HPLC. Protein was loaded onto a protein MicroTrap (Michrom Bioresources) column and washed with 0.03% TFA in water (HPLC

BIOCHEMISTRY

solution A). The protein and detergent were then separated on a reversed-phase C18 column (1 × 50 mm, Jupiter; Phenomenex) using a linear gradient of 5–60% (vol/vol) solution B (95% CH_3CN, 4.97% water, and 0.03% TFA) during 3 min.

1. Rees DC, Johnson E, Lewinson O (2009) ABC transporters: The power to change. *Nat Rev Mol Cell Biol* 10:218–227.
2. Borst P, Elferink RO (2002) Mammalian ABC transporters in health and disease. *Annu Rev Biochem* 71:537–592.
3. van Veen HW, et al. (1996) Multidrug resistance mediated by a bacterial homolog of the human multidrug transporter MDR1. *Proc Natl Acad Sci USA* 93:10668–10672.
4. Lubelski J, Konings WN, Driessen AJ (2007) Distribution and physiology of ABC-type transporters contributing to multidrug resistance in bacteria. *Microbiol Mol Biol Rev* 71:463–476.
5. Geourjon C, et al. (2001) A common mechanism for ATP hydrolysis in ABC transporter and helicase superfamilies. *Trends Biochem Sci* 26:539–544.
6. Seeger MA, van Veen HW (2009) Molecular basis of multidrug transport by ABC transporters. *Biochim Biophys Acta* 1794:725–737.
7. Chen J, Lu G, Lin J, Davidson AL, Quiocho FA (2003) A tweezers-like motion of the ATP-binding cassette dimer in an ABC transport cycle. *Mol Cell* 12:651–661.
8. Smith PC, et al. (2002) ATP binding to the motor domain from an ABC transporter drives formation of a nucleotide sandwich dimer. *Mol Cell* 10:139–149.
9. Zaitseva J, Jenewein S, Jumpertz T, Holland IB, Schmitt L (2005) H662 is the linchpin of ATP hydrolysis in the nucleotide-binding domain of the ABC transporter HlyB. *EMBO J* 24:1901–1910.
10. Orelle C, Dalmas O, Gros P, Di Pietro A, Jault JM (2003) The conserved glutamate residue adjacent to the Walker-B motif is the catalytic base for ATP hydrolysis in the ATP-binding cassette transporter BmrA. *J Biol Chem* 278:47002–47008.
11. Urbatsch IL, Tyndall GA, Tombline G, Senior AE (2003) P-glycoprotein catalytic mechanism: Studies of the ADP-vanadate inhibited state. *J Biol Chem* 278:23171–23179.
12. Aller SG, et al. (2009) Structure of P-glycoprotein reveals a molecular basis for poly-specific drug binding. *Science* 323:1718–1722.
13. Dawson RJ, Locher KP (2006) Structure of a bacterial multidrug ABC transporter. *Nature* 443:180–185.
14. Ward A, Reyes CL, Yu J, Roth CB, Chang G (2007) Flexibility in the ABC transporter MsbA: Alternating access with a twist. *Proc Natl Acad Sci USA* 104:19005–19010.
15. Oancea G, et al. (2009) Structural arrangement of the transmission interface in the antigen ABC transport complex TAP. *Proc Natl Acad Sci USA* 106:5551–5556.
16. Serohijos AW, et al. (2008) Phenylalanine-508 mediates a cytoplasmic-membrane domain contact in the CFTR 3D structure crucial to assembly and channel function. *Proc Natl Acad Sci USA* 105:3256–3261.
17. Borbat PP, et al. (2007) Conformational motion of the ABC transporter MsbA induced by ATP hydrolysis. *PLoS Biol* 5:e271.
18. Gottesman MM, Ambudkar SV, Xia D (2009) Structure of a multidrug transporter. *Nat Biotechnol* 27:546–547.
19. Kerr ID, Jones PM, George AM (2010) Multidrug efflux pumps: The structures of prokaryotic ATP-binding cassette transporter efflux pumps and implications for our understanding of eukaryotic P-glycoproteins and homologues. *FEBS J* 277:550–563.
20. Dalmas O, et al. (2005) The Q-loop disengages from the first intracellular loop during the catalytic cycle of the multidrug ABC transporter BmrA. *J Biol Chem* 280:36857–36864.
21. Pagant S, Brovman EY, Halliday JJ, Miller EA (2008) Mapping of interdomain interfaces required for the functional architecture of Yor1p, a eukaryotic ATP-binding cassette (ABC) transporter. *J Biol Chem* 283:26444–26451.
22. Zhang Z, Smith DL (1993) Determination of amide hydrogen exchange by mass spectrometry: A new tool for protein structure elucidation. *Protein Sci* 2:522–531.
23. Wales TE, Engen JR (2006) Hydrogen exchange mass spectrometry for the analysis of protein dynamics. *Mass Spectrom Rev* 25:158–170.
24. Konermann L, Pan J, Liu YH (2011) Hydrogen exchange mass spectrometry for studying protein structure and dynamics. *Chem Soc Rev* 40:1224–1234.
25. Morgan CR, et al. (2011) Conformational transitions in the membrane scaffold protein of phospholipid bilayer nanodiscs. *Mol Cell Proteomics* 10:M111.010876.
26. Rey M, et al. (2010) Conformational dynamics of the bovine mitochondrial ADP/ATP carrier isoform 1 revealed by hydrogen/deuterium exchange coupled to mass spectrometry. *J Biol Chem* 285:34981–34990.
27. West GM, et al. (2011) Ligand-dependent perturbation of the conformational ensemble for the GPCR β2 adrenergic receptor revealed by HDX. *Structure* 19:1424–1432.
28. Do Cao MA, et al. (2009) Probing the conformation of the resting state of a bacterial multidrug ABC transporter, BmrA, by a site-directed spin labeling approach. *Protein Sci* 18:1507–1520.
29. Steinfels E, et al. (2004) Characterization of YvcC (BmrA), a multidrug ABC transporter constitutively expressed in *Bacillus subtilis*. *Biochemistry* 43:7491–7502.
30. Ravaud S, et al. (2006) The ABC transporter BmrA from *Bacillus subtilis* is a functional dimer when in a detergent-solubilized state. *Biochem J* 395:345–353.
31. Hrycyna CA (2001) Molecular genetic analysis and biochemical characterization of mammalian P-glycoproteins involved in multidrug resistance. *Semin Cell Dev Biol* 12:247–256.
32. Kwan T, Gros P (1998) Mutational analysis of the P-glycoprotein first intracellular loop and flanking transmembrane domains. *Biochemistry* 37:3337–3350.
33. Oldham ML, Khare D, Quiocho FA, Davidson AL, Chen J (2007) Crystal structure of a catalytic intermediate of the maltose transporter. *Nature* 450:515–521.
34. Orelle C, et al. (2008) Conformational change induced by ATP binding in the multidrug ATP-binding cassette transporter BmrA. *Biochemistry* 47:2404–2412.
35. Doshi R, Woebking B, van Veen HW (2010) Dissection of the conformational cycle of the multidrug/lipidA ABC exporter MsbA. *Proteins* 78:2867–2872.
36. Zou P, Bortolus M, McHaourab HS (2009) Conformational cycle of the ABC transporter MsbA in liposomes: Detailed analysis using double electron-electron resonance spectroscopy. *J Mol Biol* 393:586–597.
37. Zou P, McHaourab HS (2009) Alternating access of the putative substrate-binding chamber in the ABC transporter MsbA. *J Mol Biol* 393:574–585.
38. Siarheyeva A, et al. (2007) Probing the molecular dynamics of the ABC multidrug transporter LmrA by deuterium solid-state nuclear magnetic resonance. *Biochemistry* 46:3075–3083.
39. Ananthaswamy N, et al. (2010) The signaling interface of the yeast multidrug transporter Pdr5 adopts a cis conformation, and there are functional overlap and equivalence of the deviant and canonical Q-loop residues. *Biochemistry* 49:4440–4449.
40. Oliveira AS, Baptista AM, Soares CM (2011) Conformational changes induced by ATP-hydrolysis in an ABC transporter: A molecular dynamics study of the Sav1866 exporter. *Proteins* 79:1977–1990.
41. Patzlaff JS, Moeller JA, Barry BA, Brooker RJ (1998) Fourier transform infrared analysis of purified lactose permease: A monodisperse lactose permease preparation is stably folded, alpha-helical, and highly accessible to deuterium exchange. *Biochemistry* 37:15363–15375.
42. le Coutre J, Kaback HR, Patel CK, Heginbotham L, Miller C (1998) Fourier transform infrared spectroscopy reveals a rigid alpha-helical assembly for the tetrameric *Streptomyces lividans* K+ channel. *Proc Natl Acad Sci USA* 95:6114–6117.
43. Sayeed WM, Baenziger JE (2009) Structural characterization of the osmosensor ProP. *Biochim Biophys Acta* 1788:1108–1115.
44. Pan Y, Piyadasa H, O'Neil JD, Konermann L (2012) Conformational dynamics of a membrane transport protein probed by H/D exchange and covalent labeling: The glycerol facilitator. *J Mol Biol* 416:400–413.
45. le Coutre J, Kaback HK (2000) Structure-function relationships of integral membrane proteins: Membrane transporters vs channels. *Biopolymers* 55:297–307.
46. Lewis HA, et al. (2010) Structure and dynamics of NBD1 from CFTR characterized using crystallography and hydrogen/deuterium exchange mass spectrometry. *J Mol Biol* 396:406–430.
47. Murakami S, Nakashima R, Yamashita E, Matsumoto T, Yamaguchi A (2006) Crystal structures of a multidrug transporter reveal a functionally rotating mechanism. *Nature* 443:173–179.
48. Toyoshima C, Mizutani T (2004) Crystal structure of the calcium pump with a bound ATP analogue. *Nature* 430:529–535.
49. Steinfels E, et al. (2002) Highly efficient over-production in *E. coli* of YvcC, a multidrug-like ATP-binding cassette transporter from Bacillus subtilis. *Biochim Biophys Acta* 1565:1–5.
50. Zhang Z, Marshall AG (1998) A universal algorithm for fast and automated charge state deconvolution of electrospray mass-to-charge ratio spectra. *J Am Soc Mass Spectrom* 9:225–233.

Supporting Information

Mehmood et al. 10.1073/pnas.1204067109

SI Results

Electrospray Mass Spectrometry of the Full-Length Protein. Because lipids and detergents either give strong signals in mass spectrometry (MS) or disturb the protein ionization in the electrospray source (1), they must be separated from the protein before reaching the source. Previous separations involved gel electrophoresis and electroelution (2), protein precipitation and resuspension in concentrated acidic solutions (3), or size exclusion chromatography after dissolution in a chloroform/methanol/acid solution (4). However, although efficient, all these methods were hardly compatible with the requirement of a fast preparation of the samples to limit as much as possible the back exchange reaction after deuterium incorporation into BmrA. Therefore, chromatographic parameters were first optimized to separate membrane lipids or n-dodecyl-β-D-maltoside (DDM) detergent from the protein using classical reversed phase chromatography (*Materials and Methods*).

Because of the cloning strategy used (5), purified BmrA was expected to contain three additional residues on its N terminus (sequence MAS<u>MPT</u>..., with the underlined residues corresponding to the beginning of the native protein) and 15 additional residues on its C terminus, including the Histidine tag (sequence ...<u>KAG</u>VDKLAAALEHHHHHH, with the underlined residues corresponding to the end of the native protein). Thus, the deconvoluted mass obtained is in very good agreement with the calculated mass of BmrA, possessing only one extra Ser amino acid on its N terminus (66,340 Da). Masses of a second peak (66,412 Da, in membranes) are also in very good agreement with the calculated mass of BmrA, with two extra amino acids on its N terminus, Ala plus Ser (66,411 Da). Therefore, the first methionine and sometimes also the second amino acids (Ala) of the N terminus of the proteins were very likely cleaved off by proteolysis during the purification process. The high quality of each spectrum reflects the efficiency of the chromatographic separation upstream of the electrospray source for either sample.

Mass Spectrometric Analyses of Peptides. To localize the difference in deuterium incorporation between the two conformations of BmrA, the protein digestion occurred at low pH and low temperature, and the peptide separations were optimized (*Materials and Methods*). This step was essential to reach a sequence coverage of the protein as large as possible with peptides as small as possible (6). However, DDM used for BmrA purification gave a very strong signal in MS. To enable observation of the mass spectra originating from the peptides, a protocol previously developed in our group for another membrane protein purified in Triton X100 was first attempted without success (7). Reversed-phase separation was then adjusted so that all peptides eluted before the detergent, at low temperature to limit deuterium back-exchange. For peptides sequencing using tandem MS, the chromatographic parameters were chosen for a good separation to facilitate their identification, and the detergent still eluted after the last peptides. For the analysis of deuterated peptides, the elution times were also shortened as much as possible to limit deuterium back-exchange. Pepsin and rhizopuspepsin (8) were used independently to digest BmrA. The pepsin digestion in solution yielded only 31 peptides, covering 45% of the BmrA sequence (Table S1). However, the use of immobilized pepsin significantly increased the number of peptides (67), and thus the sequence coverage increased to 78%. These results were obtained in the presence of 1.5 M guanidinium hydrochloride (GndCl), a denaturant concentration that was optimized after

different trials between 0.5 and 4 M. However, the low coverage of the hydrophobic transmembrane helices is presumably due to the presence of the detergent that might afford protection against the protease digestion. Immobilized rhizopuspepsin was also used for on-line digestion of BmrA. The goal was to obtain complementary sequence coverage to improve spatial resolution by the occurrence of overlapping peptides. The number of peptides and the sequence coverage were significantly lower in the transmembrane domain (TMD) in comparison with immobilized pepsin (Fig. S4 and Table S1). In the nucleotide-binding domain (NBD), the coverage seemed quite complementary to the one obtained by pepsin. However, after deuteration a significant number of peptides were lost with each protease, a phenomenon that is frequently observed in hydrogen/deuterium exchange (HDX) (9). This is due to a heterogeneous deuteration that induces a broadening of the MS signal, and thus a decrease in its intensity. The loss was much higher in the case of rhizopuspepsin, which was also less efficient than pepsin.

SI Materials and Methods

Materials. Unless specified, chemicals and pepsin were purchased from Sigma-Aldrich. DDM was purchased from Anatrace.

Site-Directed Mutagenesis and Purification of BmrA. Protein concentrations were estimated by using a modified Lowry method (10) for BmrA-enriched membranes, or the Bradford method (11) after purification. The accurate masses of the purified mutant and wild-type proteins were checked using electrospray MS.

Pepsin Digestion. All protein digestions in solution were performed in an ice bath at 0 °C. Protease solutions were prepared in 500 mM glycine (pH 2.2) and cooled to 0 °C. BmrA was digested in the same buffer for 2–5 min using a protease/substrate ratio of 1:1 or 1:10 (wt/wt) for pepsin and rhizopuspepsin, respectively. Increase in digestion time did not have any effect on the proteolysis. On-line digestions in the presence of 0.5–4 M GndCl were also performed in an ice bath at 0 °C using columns packed with rhizopuspepsin or pepsin immobilized on POROS-AL resin (8).

Limited Proteolysis of BmrA. BmrA was submitted to trypsin digestion at a protease/substrate ratio of 1:1,000 (wt/wt). For BmrA solubilized in detergent a reaction mixture of 100 μL was prepared, and aliquots of 10 μL were withdrawn after 5, 15, and 30 min. For the vanadate-inhibited state, 5 mM ATP, 5 mM MgCl$_2$, and 3 mM vanadate were added to the protein solution and incubated for 15 min at room temperature before adding trypsin. For digestion of BmrA-enriched membranes, a reaction mixture of 100 μL was prepared, and aliquots of 10 μL were withdrawn after 5, 15, and 30 min, 1 h, 2 h, and 3 h. Each aliquot was acidified with 1 μL of 5% TFA and immediately frozen in liquid nitrogen. SDS/PAGE (12.5%) was resolved, followed by Coomassie blue staining.

HDX of BmrA. The vanadate-inhibited state of the wild-type BmrA was prepared as above for limited proteolysis experiments. The E504A mutant was first incubated for 10 min with 5 mM ATP and 5 mM MgCl$_2$.

ATPase Activity. To measure the ATPase activity of BmrA in detergent, an enzymatic coupled assay system was used, in the presence of 0.05% DDM and as described previously (12). The activity was measured in the presence of 10–20 μg of BmrA and followed at 37 °C for 10 min. When vanadate was present, it was

added at a final concentration of 3 mM from a 100-mM stock solution (see ref. 12).

Calculation of Accessibility Areas of Peptides. The solvent accessibility area of BmrA peptides was calculated with the help of naccess. This software, based on the method of Lee and Richards (13), calculates the solvent-accessible area of a protein structure in a Protein Data Bank (PDB) format. Then, on the basis of the accessibility of each atom, the total access area of the main chain atoms was determined. To compare the solvent accessibility values with HDX MS data, the mean solvent accessibility area of individual peptides was determined by taking into account the main chain atoms only. Because region from residue 325 to residue 332 shows the most solvent-accessible surface in both models, the values for all other peptides were normalized considering the peptide 325–332 as a 100% solvent-accessible region.

Molecular Dynamics (MD) Simulations. MD trajectories were simulated with version 2.7 of NAMD (14), using the CHARMM27 force field with CMAP corrections (15), and the TIP3 (transferable intermolecular three-point) model for water molecules (16). All of the simulations were performed in the NpT ensemble. The pressure was maintained at 1 atm using a Nose-Hoover Langevin piston control (17), with period of 100 fs and damping time constant of 50 fs. Temperature was maintained at 300 K by coupling to a Langevin thermostat, with damping coefficient of 5 ps^{-1}. Electrostatic interactions were treated by the Particle Mesh Ewald algorithm (18), with grid spacing lower than 1 Å. Smoothed cutoff (10–12 Å) was used for the van der Waals interactions. Equations of motion were integrated with a time step of 2 fs. The SETTLE algorithm was used to restrain hydrogen atoms (19).
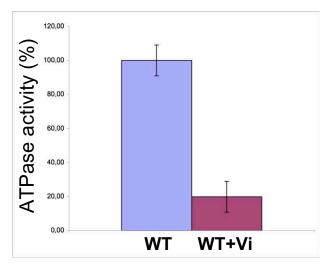
Three systems were considered: (*i*) the Sav1866 multidrug transporter from *Staphylococcus aureus* at 3.0 Å in an outward-facing conformation reflecting the ATP-bound state (20), (*ii*) the MsbA lipid "flippase" either from *Escherichia coli* in the open apo-conformation at 5.3 Å, or (*iii*) from *Salmonella typhimurium* in the outward-facing conformation at 3.7 Å (21). The structures were defined according to PDB files 2HYD, 3B5W, and 3B60,

respectively, together with the crystallographic water molecules. Only the Cα-trace structure is available in 3B5W. Missing backbone and side-chain atoms were predicted using MAXSPROUT (22) and SCWRL (23). An acetyl group was attached to the N terminus residue to mimic the preceding peptide bond, and the C-terminal carboxylate was protonated. Default ionization states at pH 7 were set, except for buried residues whose ionization states were determined using WHATIF (24) and visual inspection. The proteins were centered in the *x*–*y* plane, with the permeation pathway aligned to the *z* axis, and embedded in a preequilibrated bilayer of 569 1,2-dioleoyl-sn-glycero-3-phosphocholine (DOPC) molecules. The upper layer of the lipid membrane was aligned to the center of mass along *z* of the aromatic residues of the extracellular side (Phe158, Phe157, Tyr39, and Tyr268 in Sav1866, and Trp165, Trp66, Tyr162, Tyr168, Phe157, Phe265, and Phe272 in MsbA). Lipid molecules closer than 1.2 Å to protein atoms were removed. Sodium and chloride ions were added to neutralize the system (up to a final concentration of 150 mM). The final systems contain ~195,000 atoms in the Sav1866 simulation (~41,800 TIP3P water molecules, 360 DOPC lipids, 61Cl$^-$ and 59Na$^+$), ~202,000 atoms in the simulation of MsbA PDB 3B60 (~42,800 TIP3P water molecules, 402 DOPC lipids, 55Cl$^-$ and 63Na$^+$), and ~244 atoms in the simulation of MsbA PBD 3B5W (~53,500 TIP3P water molecules, 472 DOPC lipids, 71Cl$^-$ and 79Na$^+$).

To equilibrate the atoms around the transporters, 2,000 steps of energy minimization and 1 ns of MD were performed with restraints applied to the backbone atoms of the protein. Restraints were initially set to 10 kcal*mol^{-1}*Å^{-2}, and gradually reduced to zero. Unrestrained MD simulation followed for ~82 ns (MsbA 3B5W), ~88 ns (MsbA 3B60), and ~93 ns (Sav1866). The atomic systems used for the analyses were from the last 20 ns of the unrestrained MD. A significant drift that stabilizes at 6.7 ± 0.2 Å after 60 ns and remains constant until the end of the simulation is observed in the rmsd of MsbA (3B5W). The rmsd values of the MsbA (3B60) and Sav1866 simulations reached a plateau in less than 3 ns, with average values of 2.4 ± 0.1 Å and 1.9 ± 0.1, respectively.

1. Barnidge DR, Dratz EA, Jesaitis AJ, Sunner J (1999) Extraction method for analysis of detergent-solubilized bacteriorhodopsin and hydrophobic peptides by electrospray ionization mass spectrometry. *Anal Biochem* 269:1–9.
2. le Maire M, Deschamps S, Møller JV, Le Caer JP, Rossier J (1993) Electrospray ionization mass spectrometry on hydrophobic peptides electroeluted from sodium dodecyl sulfate-polyacrylamide gel electrophoresis application to the topology of the sarcoplasmic reticulum Ca2+ ATPase. *Anal Biochem* 214:50–57.
3. Whitelegge JP, Gundersen CB, Faull KF (1998) Electrospray-ionization mass spectrometry of intact intrinsic membrane proteins. *Protein Sci* 7:1423–1430.
4. Whitelegge JP, et al. (1999) Toward the bilayer proteome, electrospray ionization-mass spectrometry of large, intact transmembrane proteins. *Proc Natl Acad Sci USA* 96:10695–10698.
5. Steinfels E, et al. (2004) Characterization of YvcC (BmrA), a multidrug ABC transporter constitutively expressed in Bacillus subtilis. *Biochemistry* 43:7491–7502.
6. Zhang Z, Smith DL (1993) Determination of amide hydrogen exchange by mass spectrometry: A new tool for protein structure elucidation. *Protein Sci* 2:522–531.
7. Rey M, et al. (2010) Conformational dynamics of the bovine mitochondrial ADP/ATP carrier isoform 1 revealed by hydrogen/deuterium exchange coupled to mass spectrometry. *J Biol Chem* 285:34981–34990.
8. Rey M, et al. (2009) Recombinant immobilized rhizopuspepsin as a new tool for protein digestion in hydrogen/deuterium exchange mass spectrometry. *Rapid Commun Mass Spectrom* 23:3431–3438.
9. Marcoux J, et al. (2010) p47phox molecular activation for assembly of the neutrophil NADPH oxidase complex. *J Biol Chem* 285:28980–28990.
10. Bensadoun A, Weinstein D (1976) Assay of proteins in the presence of interfering materials. *Anal Biochem* 70:241–250.
11. Bradford MM (1976) A rapid and sensitive method for the quantitation of microgram quantities of protein utilizing the principle of protein-dye binding. *Anal Biochem* 72:248–254.

12. Galián C, et al. (2011) Optimized purification of a heterodimeric ABC transporter in a highly stable form amenable to 2-D crystallization. *PLoS ONE* 6:e19677.
13. Lee B, Richards FM (1971) The interpretation of protein structures: Estimation of static accessibility. *J Mol Biol* 55:379–400.
14. Phillips JC, et al. (2005) Scalable molecular dynamics with NAMD. *J Comput Chem* 26:1781–1802.
15. MacKerell AD, et al. (1998) All-atom empirical potential for molecular modeling and dynamics studies of proteins. *J Phys Chem B* 102:3586–3616.
16. Jorgensen WL, Chandresekhar J, Madura JD, Impey RW, Klein ML (1983) Comparison of simple potential functions for simulating liquid water. *J Chem Phys* 79:926–935.
17. Feller SE, Zhang YH, Pastor RW, Brooks BR (1995) Constant-pressure molecular dynamics simulation—the langevin piston method. *J Chem Phys* 103:4613–4621.
18. Essmann U, et al. (1995) A smooth particle mesh Ewald method. *J Chem Phys* 103:8577–8593.
19. Miyamoto S, Kollman PA (1992) Settle: An analytical version of the Shake and Rattle algorithm for wigid water molecules. *J Comput Chem* 13:952–962.
20. Dawson RJ, Locher KP (2006) Structure of a bacterial multidrug ABC transporter. *Nature* 443:180–185.
21. Ward A, Reyes CL, Yu J, Roth CB, Chang G (2007) Flexibility in the ABC transporter MsbA: Alternating access with a twist. *Proc Natl Acad Sci USA* 104:19005–19010.
22. Holm L, Sander C (1991) Database algorithm for generating protein backbone and side-chain co-ordinates from a C alpha trace application to model building and detection of co-ordinate errors. *J Mol Biol* 218:183–194.
23. Canutescu AA, Shelenkov AA, Dunbrack RL, Jr. (2003) A graph-theory algorithm for rapid protein side-chain prediction. *Protein Sci* 12:2001–2014.
24. Vriend G (1990) WHAT IF: A molecular modeling and drug design program. *J Mol Graph* 8:52–56, 29.

Fig. S1. ATPase activity of the wild-type BmrA. BmrA (10–20 μg) was injected into an ATPase assay medium in the absence (blue bar, WT) or presence of 3 mM vanadate (purple bar, WT + Vi). One hundred percent of ATPase activity corresponded to 1 μmol of ATP hydrolyzed/min/mg protein.
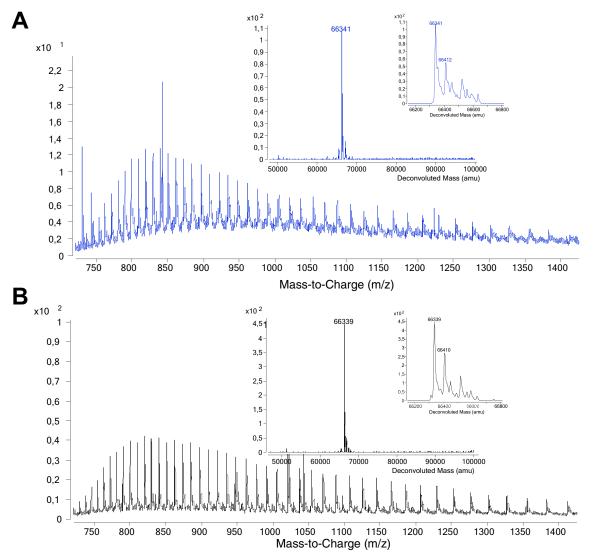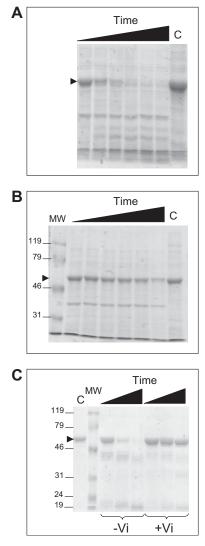

Fig. S2. Raw mass spectra of BmrA in membranes (*A*) or BmrA purified in DDM (*B*). Deconvoluted mass spectra are presented in *First Insets* with a close-up view in *Second Insets*.

Fig. S3. SDS/PAGE of BmrA-enriched membranes or BmrA purified in DDM and after limited proteolysis with trypsin. BmrA in membranes in the apo conformation (*A*) or in the vanadate-inhibited conformation (*B*) and after incubation with trypsin for 5 min, 15 min, 30 min, 1 h, 2 h, and 3 h (from left to right lanes); (*C*) BmrA purified in detergent in the apo conformation (lanes 3–5) and in the vanadate-inhibited conformation (lanes 6–8) and after incubation with trypsin for 5, 15, and 30 min (from left to right lanes). *C* is the control lane with no trypsin added, with the black arrowhead showing the position of the full-length BmrA. The masses of the molecular weight markers (MW) are indicated in kDa.
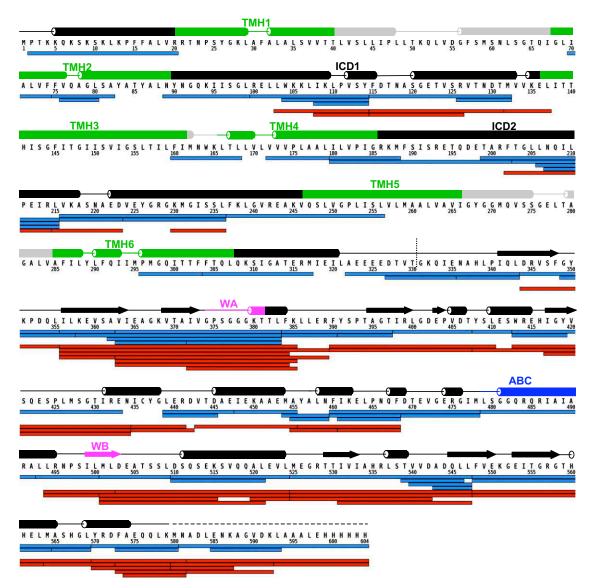
Fig. S4. Peptide mapping of BmrA using immobilized pepsin (blue) or immobilized rhizopuspepsin (red). The predicted secondary structure (cylinders for α-helices and arrows for β-strands) and topology of BmrA based on the Sav1866 3D structure is shown above the sequence with the specific regions: Walker A (WA) and B (WB) motifs and the ATP-binding cassette signature. The transmembrane helices 1–6 (TMH1 to -6) are shown in green, and the positions of the intracellular domains 1 and 2 (ICD1 and ICD2, respectively) are indicated. The extracellular parts of BmrA are shown in gray. The boundary between the TMD and the NBD is shown by a vertical dotted line. The figure was drawn with the help of the MS Tools application (1).

1. Kavan D, Man P (2011) MSTools—Web based application for visualization and presentation of HXMS data. *Int J Mass Spectrom* 302:53–58.
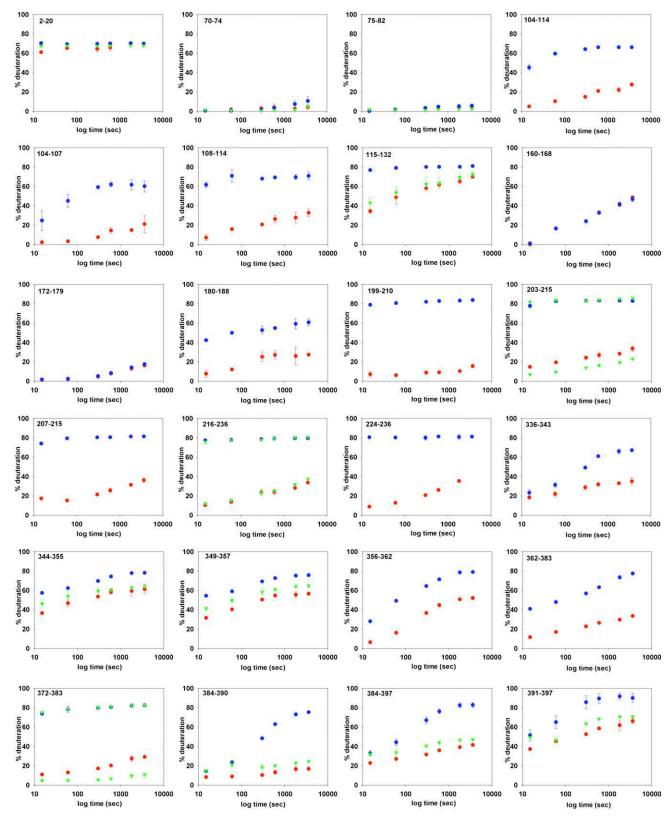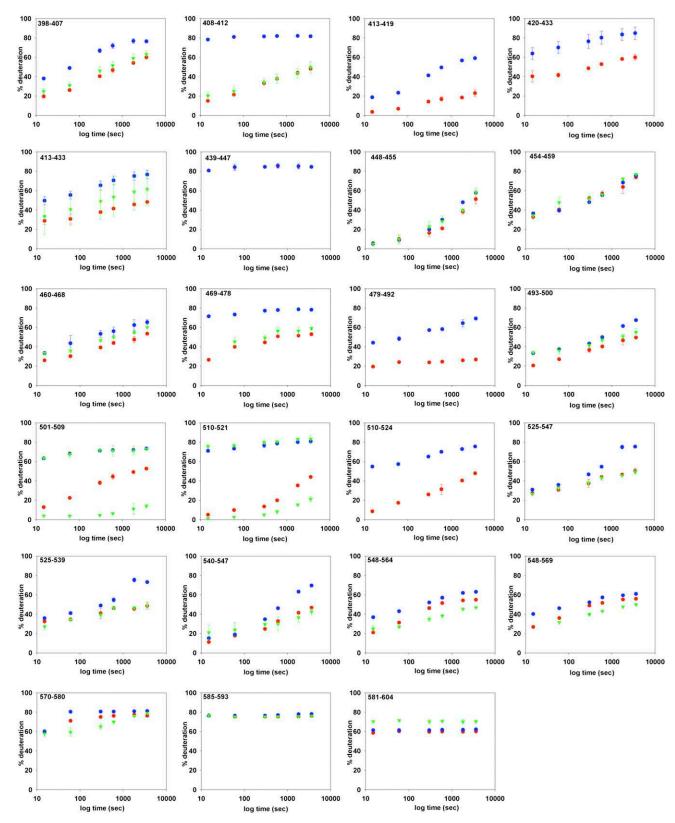
Fig. S5. (Continued)

Fig. S5. HDX kinetics of all BmrA peptides identified after digestion with immobilized pepsin. The percentage of deuteration is plotted against different deuteration times for the wild-type BmrA in the apo state (blue circles), in the vanadate-inhibited state (green triangles), or in the mutated (E504A) form (red circles). SDs (for two experiments) are shown by vertical bars; in many cases, bars are so small that they are hidden by the symbols; in the vanadate-inhibited state, the first isotopic envelope was sometimes too tiny or too close to the second one to be deconvoluted, and the kinetics could not be drawn with certainty.
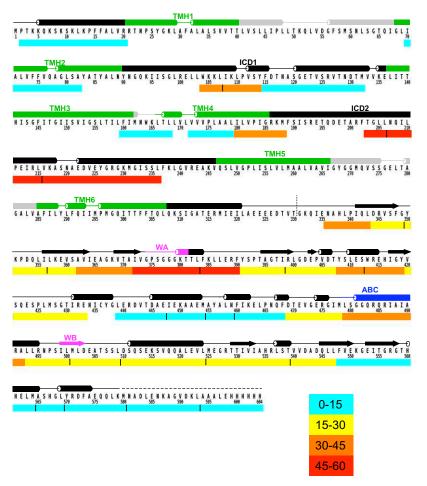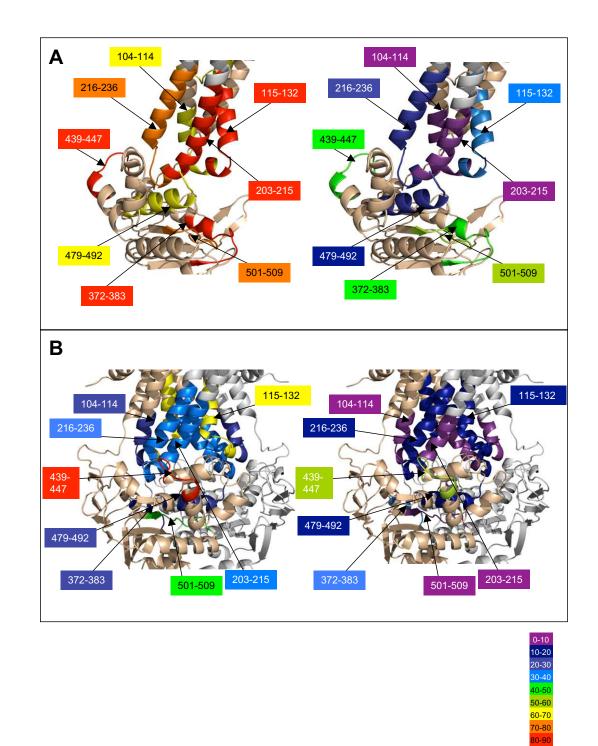
Fig. S6. Heat map showing the difference in deuterium incorporation between the apo conformation (wild-type in the resting state) and the closed conformation (E504A in the presence of ATP) after 1 h deuteration. The predicted secondary structure and topology of BmrA (see legend to Fig. S4) is indicated above the sequence. Colors defined in key at lower right.

Fig. S7. Comparison of deuterium incorporation and solvent accessibility areas in both conformations of BmrA, open (*A*) or closed (*B*). Panels at *Left* are identical to those shown in Fig. 3 for the HDX, except that only the selected peptides are colored according to the deuterium exchange scale. *Right*: Solvent accessibility of the corresponding peptides deduced from each BmrA model and using naccess software (details in *SI Materials and Methods*).
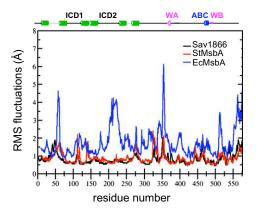
Fig. S8. Root mean square fluctuation of the Cα of Sav1866, StMsbA, and EcMsbA. Molecular dynamics simulations were performed on each structure and, once equilibrium was reached, the rms fluctuation in Å was calculated for the last 20 ns and is shown as a function of the residue number. The predicted topology of BmrA is also shown on top of the figure for comparison (see legend to Fig. S4 for color coding).

Table S1. Sequence coverage, number of peptides, and average size of the peptides for BmrA and for its domains TMD and NBD obtained in different digestion conditions and after deuteration and digestion with immobilized pepsin

Condition	BmrA	TMD	NBD
Pepsin column			
% coverage	78	60	98
Peptides	67	24	43
Average	7.0	8.0	6.4
Pepsin in solution			
% coverage	45	11	82
Peptides	31	3	28
Average	8.7	12.6	8.3
Rhizopuspepsin column			
% coverage	50	10	84
Peptides	52	8	44
Average	5.8	8.0	5.4
HDX			
% coverage	67.5	45	92
Peptides	44	15	29
Average	9.3	9.0	9.3